Evidence for antiferromagnetic ground state of Zr_2TiAl: First principles study.

P. V. Sreenivasa Reddy and V. Kanchana*

Department of Physics, Indian Institute of Technology Hyderabad, Kandi-502 285, Sangareddy, Telangana, India

G. Vaitheeswaran

Advanced Centre of Research in High Energy Materials (ACRHEM), University of Hyderabad, Prof. C. R. Rao Road, Gachibowli, Hyderabad 500 046, Telangana, India.

Andrei V. Ruban

Department of Materials Science and Engineering, Applied Materials Physics Division, Royal Institute of Technology (KTH), Stockholm, Sweden
Materials Center Leoben Forschung GmbH, A-8700 Leoben, Austria

N. E. Christensen

Department of Physics and Astronomy, Aarhus University, DK-8000 Aarhus C, Denmark.

E-mail: kanchana@iith.ac.in

Abstract. A detailed study on the ternary Zr-based intermetallic compound Zr_2TiAl has been carried out using first principles electronic structure calculations. From the total energy calculations, we find an antiferromagnetic $L1_1$-like (AFM) phase with alternating (111) spin-up and spin-down layers to be a stable phase among some others with magnetic moment on Ti being $1.22\mu_B$. The calculated magnetic exchange interaction parameters of the Heisenberg Hamiltonian and subsequent Heisenberg Monte Carlo simulations confirm that this phase is the magnetic ground structure with Neel temperature between 30 and 100 K. The phonon dispersion relations further confirm the stability of the magnetic phase while the non-magnetic phase is found to have imaginary phonon modes and the same is also found from the calculated elastic constants. The magnetic moment of Ti is found to decrease under pressure eventually driving the system to the non-magnetic phase at around 46 GPa, where the phonon modes are found to be positive indicating stability of the non-magnetic phase. A continuous change in the band structure under compression leads to the corresponding change of the Fermi surface topology and Electronic Topological Transitions (ETT) in both majority and minority spin cases, which are also evident from the calculated elastic constants and density of states calculations for the material under compression.

Keywords: Electronic structure, Antiferromagnetic, Neel temperature, Electronic

Topological Transitions, Phonons, Pressure effect

1. Introduction

Zirconium and titanium alloys are of great interest due to a variety of structural and electronic transitions in these materials. They are widely used in aerospace industry due to their light weight, static strength, stiffness and oxidation resistance.[1, 2, 3, 4, 5, 6, 7] This especially concerns their aluminides, Zr_3Al and Ti_3Al, which are important in high temperature applications.[8, 9, 10, 11, 12]

Titanium rich and zirconium ternary aluminides can be obtained by mixing Zr_3Al and Ti_3Al. Banerjee[13] and Yang et al.[14] confirmed that the Zr atom indeed gets substituted at Ti sites in Ti_3Al. Ravi et al.[15, 16] have reported the site preference of Zr atoms in Ti_3Al and the phase stability of Ti_2ZrAl compound. Recently, Zr-rich ternary intermetallic compound Zr_2TiAl has been synthesized by Sornadurai et al. using the arc-melting, vacuum annealing technique.[17] However, no further experimental or theoretical studies have been conducted for Zr_2TiAl. These points are the main motivation of this investigation. Zr_2TiAl has X_2YZ type Heusler structure,[17] which is quite different from binary aluminides, and thus interesting physical properties can exists in this case. In particular, as is known, X_2YZ type Heusler compounds can exhibit unusual magnetic properties.[18] For instance, Cu_2MnAl and Cu_2MnSn have a high value of the saturation magnetization and Curie temperature.[19, 20]

Some Zr based compounds like $ZrMn_2$ and $ZrFe_2$ have a large magnetic moment as found for Zr, which are coupled anti-parallel to the magnetic moments of Fe and Mn. [21] The electronic structure and physical properties of the solids change under pressure leading to semi metal to metal transition, magnetic to non-magnetic nature and brittle to ductile nature etc. The magnetic moment, which is one of the physical property of the solid will vanish under pressure. In the case of 3d transition metals like Fe, Co and Ni, the magnetic moment becomes zero at 18 GPa, 150 GPa and 250 GPa respectively.[22] It is also observed that as pressure increases phase change[23] from an antiferromagnetic (AFM) phase to nonmagnetic in $CaFe_2As_2$ and AFM2 to AFM1 in $BaFe_2As_2$. In the case of CsCl-type FeSe a transition from AFM phase to NM phase is observed with intermediate FM phase.[24] In recent studies,[25] hcp Co is observed to become non-magnetic at a pressure of 180 GPa with a series of Electronic Topological Transitions (ETT) at different pressures. Non-monotonic variation of the density of states and superconducting transition temperature (T_C) [26, 27, 28, 29] is observed under pressure. Recently change in the FS topology and non-monotonic variation in the density of states and single crystalline elastic constants is found to lead to the ETT's in Nb based superconducting compounds[30] under compression. The main aim of the present paper is to study the magnetic behaviour of the present compound and its pressure dependence.

The paper is organized as follows: Section 2 presents computational details of the first-principles calculations. The results and discussions are presented in section 3. The pressure effect on varies properties of Zr_2TiAl is discussed in section 4. Finally, conclusions are presented in section 5.

2. Computational details

Several first-principles methods based on density functional theory (DFT) have been used in the present work to calculate the electronic structure, elastic constants, vibrational and magnetic properties of Zr_2TiAl. The Full-Potential Linearized Augmented Plane Wave (FP-LAPW) method as implemented in the WIEN2k [31, 32] code is used to calculate the electronic structure and Fermi surface properties with spin polarization. We have used PBE-GGA [33] (Perdew-Burke-Ernzerhof parametrization of the Generalized Gradient Approximation) approximation for the exchange correlation potential. Throughout the calculations, the R_{MT} (radius of muffin tin spheres) value for each atom was fixed as 2.39 $a.u$ for Zr atom, 2.45 $a.u$ for both Ti and Al atoms. The plane wave cut-off has been chosen to satisfy R_{MT}*K_{max}=9. The potential and charge density were Fourier expanded up to G_{max}=9 $a.u^{-1}$. All the electronic properties like density of states and the Fermi surface have been calculated using $44 \times 44 \times 44$ k-point grid of the Monkhorst-Pack [34] mesh, which yields 2168 k-points in the irreducible part of the Brillouin Zone (BZ). This ensures accurate determination of the Fermi level and ground state properties. The Brillouin zone integration have been done by the tetrahedron method[35]. The Birch-Murnaghan [36] equation of state has been used to fit the total energies as a function of primitive cell volume to obtain the bulk modulus and the equilibrium lattice parameter for the investigated compound.

Phonon dispersions and electron-phonon interaction were calculated using the plane wave ultrasoft pseudopotential method (PWSCF) which is implemented in QUANTUM ESPRESSO code.[37] The GGA-PBE exchange correlation functional is used in these calculations for all the compounds. The maximum plane wave cut-off energy (ecutwfc) was 50 Ry and the electronic charge density was expanded up to 500 Ry. Gaussian broadening of 0.01 Ry and a $4 \times 4 \times 4$ uniform grid of q-points are used for phonon calculations.

The exact muffin-tin orbital (EMTO) method [38, 39] has been used to calculate the magnetic exchange interaction parameters of the Heisenberg Hamiltonian,[40, 41, 42] as implemented in the Lyngby version of the Green's function EMTO code.[44] The self-consistent electronic structure calculations at a fixed lattice constant of 6.8 Å have been done in the local density approximation using Perdew and Wang functional,[43] as well as using the GGA-PBE one. In the Brillouin zone integration, a 20×20×20 Monkhorst-Pack grid have been used.[34] All the calculations have been done with $l_{max} = 3$ for partial waves and the electronic core states were recalculated at every iteration during the self-consistent calculations for valence electrons. The electronic structures of magnetically random systems were obtained in the coherent potential approximation (CPA).[45, 46]

3. Results and discussions

3.1. Ground state properties

In order to study the ground state properties, the total energy of Zr_2TiAl has been calculated in four different magnetic states: ferromagnetic (FM), two AFM, AFM1 and AFM2, as well as non-spin-polarized or nonmagnetic (NM) one. The calculated AFM structures are shown in Fig. 1. For AFM1, the spin orientation of Ti (111) planes is anti-parallel to each other between the adjacent Ti (111) planes (Fig. 1a). In case of AFM2, the spin orientation of first two Ti planes is parallel to each other and anti-parallel to next two Ti planes as shown in Fig. 1(b).

The total energies are shown in Fig. 2(a). As one can see, the AFM1 state has the lowest energy among the considered structures with a magnetic moment of 1.22 μ_B at Ti site. The total energy increases in the sequence: AFM1 $\rightarrow$ AFM2 $\rightarrow$ FM $\rightarrow$ NM. The energy difference between AFM1 and AFM2 is 0.76 mRy/f.u., while it is 2.22 mRy/f.u. between AFM1 and FM and 9.17 mRy/f.u. between AFM1 and NM states. This result is highly unexpected since none of the alloy components is magnetic.

The calculated lattice parameter (a) and bulk modulus values using the Birch-Murnaghan equation of state are given in Table 1. The calculated lattice parameter is in good agreement with the experiment[17]. Sieberer et. al. [47] concluded that if both LDA and GGA predict a magnetic ground state at equilibrium lattice constant, then the system is magnetic. From Table 1 we can observe that both LDA and GGA predict a magnetic moment for Ti atom in the system indicating the magnetic nature of present compound. We further performed the electronic structure calculations using the optimized lattice parameter.

3.2. Magnetic ordering from exchange interaction parameters

In order to confirm the magnetic ground state structure, we have also performed *ab initio* calculations of the magnetic exchange interaction parameters of Heisenberg Hamiltonian:

$$H = -\sum_{p} J_p \sum_{ij \in p} \mathbf{e}_i \mathbf{e}_j \tag{1}$$

using the EMTO Green's function technique.[44] Here, J_p are the magnetic exchange interactions at the coordination shell p and $\mathbf{e}_i$ is the unit vector of the direction of the magnetic moment at site i. More details regarding the method used in the magnetic exchange interaction calculations can be found in reference [48].

The calculations have been done at the fixed lattice constant of 6.83 Å, which is slightly below the room-temperature experimental one, since the magnetic phase transition is expected to be at a relatively low temperature as is the case in the present calculations. The magnetic exchange interactions on Ti sublattice have been obtained in three different magnetic states: FM, disordered local moment (DLM) paramagnetic, and AFM1 using both LDA and GGA-PBE functionals for the exchange correlation potential. The DLM paramagnetic state has been modelled by using the CPA.

In general, one can hardly expect magnetism in Zr_2TiAl to be of a Heisenberg type, when magnetic exchange interactions are independent of the magnetic configuration of the system. Even in the case of bcc Fe, magnetic exchange interactions exhibit a quite strong dependence on magnetic state.[49] Nevertheless, as one can see in Fig. 3, the magnetic interactions of Ti atoms in Zr_2TiAl are very similar in all three magnetic states, with the strongest ferromagnetic and antiferromagnetic interactions at the first and second coordination shell, respectively. This is so in spite of the fact that the magnetic moment of Ti strongly depends as on the magnetic state as well as on the exchange-correlation potential: it has the lowest value in the DLM-LDA calculations, which is 0.40 μ_B, and highest in the AFM-GGA one, which is 1.22 μ_B.

The effect of the exchange-correlation potential on the magnetic moment is quite pronounced. The GGA magnetic moments are appreciably higher than the corresponding LDA ones (for the same lattice constant, as has been indicated above). In present case GGA values for both AFM and DLM cases are 1.22 μ_B and 0.73 μ_B and the LDA values for both AFM and DLM cases are 0.94 μ_B and 0.40 μ_B respectively. This of course affects the values of the magnetic exchange interactions, which are substantially larger in the GGA calculations. Since it is not clear which functional is the best for magnetic properties, the range of interactions determines the uncertainty in the present *ab initio* calculations.

In order to identify the magnetic ground structure and the magnetic phase transition temperature, we have performed Heisenberg Monte Carlo simulations using the first 21 exchange DLM and AFM interaction parameters, both LDA and GGA, with a simulation box containing 6912 atoms of the fcc underlying lattice ($12\times12\times12(\times4)$). The lowest transition temperature, 30 K, is obtained for the DLM-LDA interactions, while the highest one, 100 K, for the DLM-GGA interactions. Both AFM-LDA and AFM-GGA interactions yield practically the same transition temperature of about 60 K. This is an interesting result taking into consideration a quite large difference between interactions. Owing to the magnetic state and exchange-correlation dependence of the magnetic exchange interactions, one can expect that Neel temperature of Zr_2TiAl is in between 30 and 100 K. It is quite low but it is consistent with the relative small total energy differences of magnetic structures presented above.

The magnetic ground state structure is AFM1 in all the cases. It has $L1_1$ structure (CuPt-type of ordering) of alternating spin-up and spin-down (111) layers in the [111] direction. The first eight spin-spin correlation functions of this structure are 0, -1, 0, 1, 0, -1, 0, 1 and its combination with the magnetic exchange interactions in Fig. 3 allows one to understand the origin of this type of magnetic ordering in Zr_2TiAl. Let us note that in the case of AFM-LDA and DLM-LDA interactions, it is not enough to consider just the first two strongest interactions in order to get the AFM1 ground state. More distant interactions provide quite substantial and decisive contribution.

Finally, we have also estimated the AFM1-FM energy difference using different sets of interactions and found that it is -1.02, -0.72, -0.30, and -0.03 mRy for the AFM-GGA, DLM-GGA, AFM-LDA, and DLM-LDA interactions, respectively. The GGA results are

in reasonable agreement with the direct total energy calculations (one should keep in mind that since magnetic exchange interactions are dependent on the magnetic state, they cannot provide accurate energy difference for two different magnetic states).

3.3. Electronic structure

The calculated band structures are given in Fig.4 for AFM1, AFM2 and FM states in the supercell as shown in Fig.1. In AFM1 case the majority and minority band structures are degenerate and we have plotted only majority spin bands in Fig.4(a). The Fermi level is aligned to 0 eV. From the band structure we have observed five bands to cross Fermi level (E_F) and are given in different colours in AFM1. Similarly, band structure of AFM2 state is given in Fig.4(b), which is almost similar to AFM1 with a change in the band structure topology along W-L and X-W-K directions where the bands are compressed near E_F in comparison with AFM1 band structure. For the same supercell FM calculations are done and the calculated majority and minority band structures are given in Fig.4(c) and 4(d). The number of bands to cross Fermi level (E_F) is different in both majority (five bands) and minority spin (four bands) cases of FM state which are indicating the non-degenerate behaviour in the band structure topology. In FM case we find absence and presence of bands near the E_F around Γ point in majority and minority spin cases respectively. For further calculations we proceed with the initial Heusler structure(with space group $Fm\bar{3}m$) as the energy difference between FM and AFM is very low.

The calculated energy bands corresponding to both majority and minority spin case for the ferro magnetic phase of Zr_2TiAl for normal Heusler structure(with space group $Fm\bar{3}m$) are shown in Fig.5(a,b) along the high symmetry directions of the cubic FCC (face centred cubic) Brillouin zone (BZ). We have observed that in both majority and minority spin channels only one band is crossing the Fermi level (E_F) and indicate the metallic nature of the investigated compound. The valence band has a band width of around 7 eV in both majority and minority spin. It may be seen that the low lying band (at -5 eV), which give rise to the low energy tail in the density of states is mainly of Al-s states. The higher lying bands in the vicinity of Fermi level are primarily Zr-d and Ti-d derived states. The band which is crossing the E_F from valence band to conduction band in the case of majority spin is of hole nature and in the case of minority spin it is having same nature with a pocket at the Γ point. From the keen observation of the band structure, we have found almost non-dispersive band just below the E_F in both majority and minority spin cases. In majority spin case it is observed along L-Γ-X and the same is observed in minority spin case along W-L and W-K directions. This feature is particularly called as van Hove singularity which might result in a peak in the electronic density of states.

Further to know the electronic density of states (DOS) at the E_F in the present investigated compound, we have calculated the total, atom projected and orbital projected density of states using tetrahedron method [35] and are given in Fig.6. For

both majority and minority spin there is a separation between bonding and anti bonding regions and the Fermi level lies in the bonding region and lies very close to the pseudo gap. The total DOS ($N(E_F)$) value for the majority spin is 2.677 $states/eV/f.u.$ and for the minority spin it is 2.630 $states/eV/f.u.$ It is evident that the low lying bands in both majority and minority spin are mainly due to Al-s orbitals as stated earlier and are well separated from the higher lying p-d band gap indicating a weak hybridization with higher bands in both majority and minority spin. From the calculated atom projected DOS, we can see that at E_F, the major contribution is from the Ti atom in the majority spin, especially Ti $d_{t_{2g}}$ states. In the minority spin especially d_{eg} states of Zr atom contribute more at the E_F. As previously discussed the peak below the E_F in majority spin case and on the E_F in the minority spin case are due to van Hove singularity in the band structure.

To analyse the Fermi surface topology of the bands which cross the E_F in both spin cases we have calculated Fermi surfaces (FS) for the corresponding bands and are shown in the Fig.5(c,d). As we already discussed, the FS for majority spin have a hole sheet (Fig.5(c)) which is due to the band crossing the E_F from valence band to conduction band along W-L and X-W-K directions as shown with dotted line in Fig.5(a). In this FS we have openings at X and L points in the BZ where the band crossing is absent in the BZ. In the case of minority spin we have single FS (Fig.5(d)) which have pocket around Γ point due to the band crossing at the same Γ point from valence band to conduction band. This Γ point pocket is covered with a sheet except at the square face of the BZ which is due to the band crossing E_F along W-L and W-K directions from valence band to conduction band which is shown with dotted line in Fig.5(b).

To discuss the bonding in the present compound, we have calculated difference charge density and spin charge density and are given in Fig.7. Pauling electro negativity values for the constituent atoms are 1.33, 1.54 and 1.61 for Zr, Ti and Al atoms respectively. There is a possibility of charge transfer from Zr and Ti to Al due to its high electro negativity values. Due to this charge transfer the Ti^{3+} state would be formed, which is due to the loss of three valence electrons and has only one free electron. Due to this free electron a possible spin magnetic moment will arise which could be a reason for the present magnetic moment at Ti site. We have also calculated the Bader charge[51] to identify the charge flow among the constituent elements as given in Table 3. The calculated values are 0.47e for each Zr atom, 0.12e for Ti and -1.07e for Al at ambient. This shows the charge flow from Zr and Ti elements to Al. As Al is the most electronegative element in this compound and will pickup 0.47e from each Zr and 0.12e from Titanium. The latter again follows from the electro negativities, as Zr is more electro positive than Ti. From the calculated spin charge density plots we can observe that the magnitude of the spin density is more at the Ti atoms site rather than other atoms. This indicates that the effect of Ti is more rather than other elements contributing to the magnetic nature in the present compound.

To check the mechanical stability of the present compound we have calculated the elastic constants for both magnetic and non-magnetic cases and are given in the Table.2

at ambient condition. The calculated single crystalline elastic constants C_{11}, C_{12} and C_{44} are found to satisfy the Born mechanical stability criteria [50] i.e. $C_{11} > 0$, $C_{44} > 0$, $C_{11} > C_{12}$, and $C_{11} + 2C_{12} > 0$, in magnetic case. But in the case of non-magnetic case these criteria are not fulfilled. This further confirms the mechanically stable nature of the present compound in magnetic case.

In order to comment on the phase stability of the investigated compound, we have calculated the phonon dispersion relations along the high symmetry directions of the Brillouin zone at ambient condition for both magnetic and non-magnetic phases illustrated in Fig.8 along with the partial phonon density of states. In each plot there are 12 phonon branches as the unit cell of Zr_2TiAl contains four atoms. There are three acoustic and nine optical branches. The absence of imaginary modes in the magnetic phase as shown in Fig.8(a) indicates the stability in the magnetic phase at ambient conditions, whereas the instability in the non-magnetic phase at ambient conditions is observed with the presence of imaginary mode along Γ- X - W direction as shown in Fig.8(b). By comparing these phonon dispersion plots in both the cases at ambient condition, frequency hardening is observed in magnetic phase rather than in non-magnetic phase. In both phases the higher frequency optical modes at nearly 265 cm^{-1} are separated with a gap of 80 cm^{-1} from other lower frequency modes. From the calculated partial phonon density of states we can say that the vibrational energies are higher in magnetic phase compared to the non-magnetic phase. Again from the partial phonon density of states, the higher frequency optical modes are due to the light Al atoms in both magnetic and non magnetic case. In the magnetic case the modes near the frequency 175 cm^{-1} are separated from higher and lower frequency branches and are due to the contribution of the Ti atoms. In lower frequency region the contribution of all atoms is same in both magnetic and non-magnetic case.

As shown and already discussed, the magnetic phase is found to be stable at ambient condition, but under pressure we find a second order phase transition from magnetic to non-magnetic phase, where we find the magnetic moment of Ti to vanish as shown in Fig.1(b) at a pressure of 46 GPa. A detailed discussion of the pressure effect on the above mentioned properties is given in the next section.

4. Pressure effect

The calculated effects of applied pressure on the band structure of Zr_2TiAl are illustrated in Fig.9 for both majority and minority spins. Here we have applied uniform compression in all the crystallographic directions. With increasing pressure the number of bands crossing E_F is increased from one to three in both spin cases upto the final compression. This indicates the Electronic topological transitions (ETT) in the present compound at different compressions. The corresponding change in the FS topology at each compression is given in the Fig.10. As pressure increases the E_F shift towards either higher or lower energy region. This shift in the E_F can cause changes in the band structure which again leads to a change in the FS topology. In our case we find E_F

to shift towards the valence region in majority spin case and towards the conduction region in the minority spin case which is evident from Fig.9. Due to this, the number of bands to cross E_F is increasing at particular pressures in both the spin cases. The topology of the FS depends on the area occupied by the band near E_F. As pressure increases, there is a change in the occupied area of the band at E_F which leads to a change in the FS topology. From Fig.10, it is observed that a continuous change in the topology of FS at all the compression along with the addition of new FS sheets at certain compressions lead to ETT's. From Fig.9, it is observed that the additional band to cross the E_F in majority spin case occurs at V/V_0=0.96 (pressure of 4.22 GPa) along Γ-X direction. Due to this, we find an additional FS which is evident from the Fig.9 at the same compression. The complete band structure at this compression is given in Fig.11 and the corresponding FS topology can be found in Fig.10. From this, we found small pockets along Γ-X in the first FS which is evident from Fig.10 at this compression compared to ambient. At the same point the second band is also found to cross the E_F which is evident from the zoomed figure from Fig.11 and the corresponding FS is shown in Fig.10. For higher compressions, the FS topology change still continues, and at V/V_0=0.92 (pressure 9.45 GPa) for minority spins two additional bands found to cross the E_F and due to this two additional FS sheets are found, see Fig.9. From Fig.12, where the complete band structure is given at this compression and corresponding FS topology can be seen in Fig.10., the changes in the band structure and FS topology are observed at L point where the new bands are added as shown from the zoomed band structure in Fig.12. The FS for these new bands are given in Fig.10. Above this compression at V/V_0=0.85 (pressure of 21 GPa) in majority spin case another band is found to cross the E_F at Γ point. Due to this an extra FS sheet is found at the Γ point which is evident from Fig.10. At the final compression V/V_0=0.75 (pressure of 46 GPa) it is found that the band structure and FS for both majority and minority spin cases is found to be same indicating the non-magnetic nature of the present compound at this compression. The complete band structure given for this compression in Fig.13 (corresponding FS can be see in Fig.10). This non-magnetic nature is again confirmed from the calculated magnetic moment of the Ti, which is found to be 0 μ_B at this compression as shown in Fig.1(b).

These changes in the FS topology are again an indication of some anomalies in the system. For further investigations we have also calculated the DOS under compression and the results are given in Fig.14(a). Non-monotonic variations in the DOS under compression in both majority spin and minority spin are found. Recently it was shown that the Fermi surface topology change and non monotonic variation in the DOS can be used to predict the ETT's in the Nb based superconducting compounds[30]. In the present compound this could be a reason for second order magnetic to non-magnetic phase transition.

To confirm the signatures of ETT's we have also calculated the single crystalline elastic constants and shear modulus ($C_s = (C_{11} - C_{12})/2$) for all the compressions and the values are plotted in Fig.14. From the above discussion, we have observed ETT's at

V/V_0=0.96(for majority spin), V/V_0=0.92(for minority spin) and V/V_0=0.85(majority spin) and in remaining compressions a continuous change in the band structure and FS topology is also observed. The ETT's due to the majority spin (V/V_0=0.96, 0.85) can be directly observed from the softening of C_s elastic constant at that compression from Fig.14(a). The remaining ETT due to the minority spin (V/V_0=0.92) is not observed directly form the C_s but it can be observed form the calculated total DOS in minority spin case at that compression where we can see the decrease in the total DOS value from Fig. 14(a). A sudden drop in the total magnetic moment is observed at V/V_0=0.92 and 0.85 due to complete occupancy of minority spin at V/V_0=0.92 and majority spin case at V/V_0=0.85. The resulting decrease in the magnetic moment is the primary reason for the destabilization of magnetic phase in Zr_2TiAl at high compressions. Again to confirm the non-magnetic phase at V/V_0=0.75 we have calculated the phonon dispersion relations at the same compression and they are given in Fig.8(b) (red coloured dotted line), where we observed the phonon hardening and the disappearance of imaginary mode.

5. Conclusions

We have investigated the electronic, magnetic, elastic, and vibrational properties of the Zr_2TiAl compound at ambient pressure as well as under compression. The obtained structural parameters are in good agreement with the existing experimental data. We have determined that Zr_2TiAl has antiferromagnetic ground state with ordering spin-up and spin-down Ti (111) layers with the magnetic moment of Ti atoms 1.22 μ_B. The magnetic ground state is also confirmed in the Monte Carlo simulations using different sets of magnetic exchange interactions. The theoretically determined Neel temperature is between 30 to 100 K depending on the exchange correlation functional. The stability of the magnetic phase is also confirmed from the calculated elastic constants and phonon dispersion relations. We have also observed the magnetic to non-magnetic phase transition under compression due to the disappearance of the Ti magnetic moment, which tends to zero at V/V_0=0.75 ($\approx$ 46 GPa). Three ETT's are observed at V/V_0=0.96, 0.92 and 0.85, due to which a sudden drop in the magnetic moment of Ti atom is observed under compression.

6. Acknowledgement

The authors would like to thank Department of Science and Technology (DST) for the financial support through SR/FTP/PS-027/2011. The authors would also like to acknowledge IIT-Hyderabad for providing the computational facility. AVR acknowledges the support of the Swedish Research Council (VR project 2015-05538), the European Research Council grant, the VINNEX center Hero-m, financed by the Swedish Governmental Agency for Innovation Systems (VINNOVA), Swedish industry, and the Royal Institute of Technology (KTH). Calculations have been done using

NSC (Linköping) and PDC (Stockholm) resources provided by the Swedish National Infrastructure for Computing (SNIC). The support by the Austrian Federal Government (in particular from Bundesministerium für Verkehr, Innovation und Technologie and Bundesministerium für Wirtschaft, Familie und Jugend) represented by Österreichische Forschungsförderungsgesellschaft mbH and the Styrian and the Tyrolean Provincial Government, represented by Steirische Wirtschaftsförderungsgesellschaft mbH and Standortagentur Tirol, within the framework of the COMET Funding Programme is also gratefully acknowledged. V.K and G.V are greatly indebted to their departed collaborator Axel Svane for fruitful discussion during the initial stage of this project.

[1] Duthi J and Pettifor D 1977 *Phys. Rev. Lett.* **38**, 564
[2] Skriver H 1985 *Phys. Rev. B* **31** 1909
[3] Gyanchandani J, Gupta S, Sikka S and Chidambaram R 1990 *J. Phys.: Condens. Matter* **2** 6457
[4] Gyanchandani J, Gupta S, Sikka S and Chidambaram R 1990 *J. Phys.: Condens. Matter* **2** 301
[5] Kutepov A L and Kutepova S G 2003 *Phys. Rev. B* **67** 132102
[6] Ahuja R, Dubrovinsky L, Dubrovinskaia N, Osorio Gullen J M, Mattesini M, Johansson B and Le Bihan T 2004 *Phys. Rev. B* **69** 184102
[7] Yan-Jun Hao, Lin Zhang, Xiang-Rong Chen, Ying-Hua Li and Hong-Liang He 2008 *J. Phys.: Condens. Matter* **20** 235230
[8] Nihat Arikan 2013 *J. Phys. Chem. Solids* **74** 794-798
[9] Geist D, Rentenberger C and Karnthaler H P 2008 *Material Science Forum* **584-586** 553-558
[10] Ravindran P and Asokamani R 1994 *Phys. Rev. B* **50** 668-678
[11] Hong T, Watson-Yang T J, Guo X -Q, Freeman A J and Oguchi T 2000 *Phys. Rev. B* **43** 1940-1947
[12] Dubrovinskaia N A, Vennstrom M, Abrikosov I A, Ahuja R, Ravindran P, Andersson Y, Eriksson O, Dmitriev V and DUbrovinsky L S 2000 *Phys. Rev. B* **63** 024106
[13] Banerjee D, in Intermetallic Compounds-Principles and Practice 2, edited by J. H. Westbrook and R. L. Fleischer 101 (Wiley, NewYork, 1995), p. 101.
[14] Yang R, Hao Y L and Li D(unpublished)
[15] Ravi C, Mathijaya S, Valsakumar M C and Asokamani R 2002 *Phys. Rev. B* **65** 115188
[16] Ravi C, Vajeeston P, Mathijaya S and Asokamani R 1999 *Phys. Rev. B* **60** 683-690
[17] Sournadurai D, Sastry V S, Thomas Paul V, Roberta Flemming, Feby Jose, Rameshan R and Dash S 2012 *Intermetallics* **24** 89-94
[18] Webster P J and Ziebeck K R A 973 *J. Phys. Chem. Solids.* **34** 1647
[19] Heusler F 1903 *Verh Disch Phys Ges* **5** 219
[20] Heusler F, Stark W and Haupt E 1905 *Vehandl. Deut. Physik. Ges.* **5** 220
[21] Suklyun Hong and Fu C L 2002 *Phys. Rev. B* **66** 094109
[22] Valentin lota, Jae-Hyun Park Klepeis, Choong-Shik Yoo, Jonathan Lang, Daniel Haskel and George Srajer 2007 *Appl. Phys. Lett.* **90** 042505
[23] Yanli Wang, Yi Ding and Jun Ni 2009 *Solid. State. Commn.* **149** 2125-2129
[24] Gul Rahman, In Gee Kim and Freeman A J 2010 *J. Magn. Magn. Mater* **322** 3153-3158
[25] Kvashnin Y O, Sun W, Di Marco I and Eriksson O 2015 *Phys. Rev. B* **92** 134422
[26] Ram S, Kanchana V, Vaitheeswaran G, Svane A, Dugdale S B and Christensen N E 2012 *Phys. Rev. B* **85** 174531
[27] Ram S, Kanchana V, Svane A, Dugdale S B and Christensen N E 2013 *J. Phys.: Condens. Matter* **25** 155501
[28] Sreenivasa Reddy P V and Kanchana V 2014 *J. Alloys. Compd.* **616** 527-534
[29] Sreenivasa Reddy P V, Kanchana V, Vaitheeswaran G and Singh D J 2016 *J.Phys.:Condens. Matter* **28** 115703
[30] Sreenivasa Reddy P V, Kanchana V, Vaitheeswaran G, Modak P and Verma A K 2016 *J. Appl. Phys.* **119** 075901
[31] Blaha P, Scwarz K, Sorantin P and Tricky S B 1990 *Comput. Phys. Commun.* **59** 399-415
[32] Blaha P, Scwarz K, Madsen G K H, Kvasnicka D, Luitz J, In: K. Schwarz, editor. *WIEN2k, an augumented plane wave plus local orbital programe for calculating crystal properties.* Austria: Tech. Techn. Universität Wien, Austria, ISBN 3-9501031-1-2;2001.
[33] Perdew J P, Burke K and Ernzerhof M 1996 *Phys. Rev. Lett.* **77** 3865
[34] Monkhorst H J and Pack J D 1976 *Phys. Rev. B* **13** 5188
[35] Blochi P E, Jepsen O and Andersen O K *Phys. Rev. B* **49** 16223
[36] Birch F 1947 *Phys. Rev.* **71** 809
[37] Giannozzi P, Baroni S, Bonini N, Calandra M, Car R, Cavazzoni C, Ceresoli D, Chiarotti G L, Cococcioni M, Dabo I, Corso A D, de Gironcoli S, Fabris S, Fratesi G, Gebauer R, Gerstmann

U, Gougoussis C, Kokalj A, Lazzeri M, Martin-Samos L, Marzari N, Mauri F, Mazzarello R, Paolini S, Pasquarello A, Paulatto L, Sbraccia C, Scandolo S, Sclauzero G, Seitsonen A P, Smogunov A, Umari P and Wentzcovitch R M 2009 *J. Phys.: Condens. Matter* **21** 395502

[38] Andersen O K, Jepsen O and Krier G: In V. Kumar, Andersen O K and Mookerjee A (eds.) *Lectures on Methods of Electronic Structure Calculations* (World Scientific Publishing Co., Singapore, 1994), p. 63.

[39] Vitos L, *Computational Quantum Mechanics for Materials Engineers* (Springer-Verlag, London, 2007).

[40] Oguchi T, Terakura K and Hamada H 1983 *J. Phys. F: Met. Phys.* **13** 145; Oguchi T, Terakura K and Williams A R 1983 *Phys. Rev. B* **28** 6443

[41] Liechtenstein A, Katsnelson M I and Gubanov V A 1984 *J. Phys. F: Met. Phys.* **14** L125

[42] Liechtenstein A, Katsnelson M I, Antropov V P and Gubanov V A 1987 *J. Magn. Magn. Mat.* **67** 65

[43] Perdew J P and Wang Y 1992 *Phys. Rev. B* **45** 13244

[44] Ruban A V and Dehghani M 2016 *Phys. Rev. B* **94** 104111

[45] Soven P 1967 *Phys. Rev.* **156** 809

[46] Gyorffy B L 1972 *Phys. Rev. B* **5** 2382

[47] Sieberer M, Khmelevskyi S and Mohn P *Phys. Rev. B* **74** 014416

[48] Ruban A V and Dehghani M 2016 *Phys. Rev. B* **94** 104111

[49] Ruban A V, Shallcross S, Simak S I and Skriver H L 2004 *Phys. Rev. B* **70** 125115

[50] Born M 1939 *J. of Chem. Phys.* **7** 591

[51] Bader R F W *Atoms in Molecules: A Quantum Theory*, International Series of Monographs on Chemistry (Oxford University Press, Oxford, 1990), Vol. 22.

Table 1. Ground state properties of Zr_2TiAl at ambient pressure combined with experimental reports.

Parameters	LDA	LDA-mag	GGA	GGA-mag	Experimental[17]
Lattice parameter a (Å)	6.668	6.712	6.813	6.841	6.8400
Bulk modulus B (GPa)	115	110	102	97	–
Magnetic moment of Ti τ (μ_B)	–	0.8	–	1.22	–

Table 2. Calculated elastic constants at ambient condition for both magnetic and non-magnetic phases.

Parameters	Magnetic case	Non-magnetic case	Experiment
C_{11} (GPa)	109	94	-
C_{12} (GPa)	90	100	-
C_{44} (GPa)	58	53	-

Table 3. Calculated Bader charge for all the compressions.

V/V_0	Zr1	Zr2	Ti	Al
1.00	0.47	0.47	0.12	-1.07
0.98	0.46	0.46	0.13	-1.06
0.96	0.45	0.45	0.14	-1.05
0.94	0.44	0.44	0.15	-1.04
0.92	0.42	0.42	0.17	-1.01
0.90	0.41	0.41	0.18	-0.99
0.85	0.36	0.36	0.21	-0.93
0.80	0.30	0.30	0.24	-0.83
0.75	-0.01	-0.01	0.48	-0.46

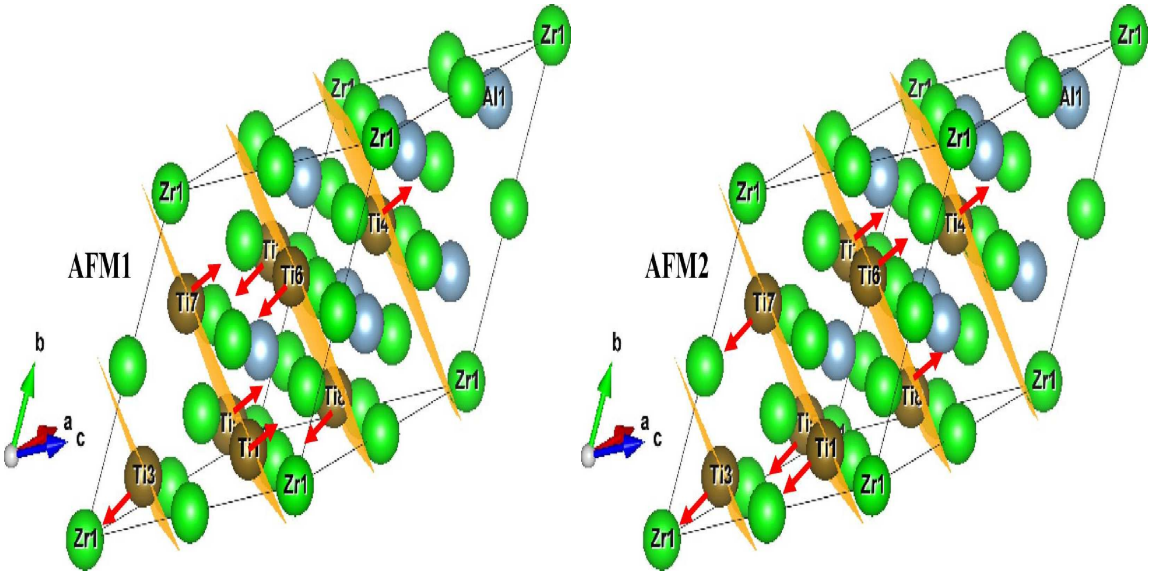

(a) (b)

Figure 1. Calculated AFM structures: (a) AFM1: Anti-parallel spin alignment between two Ti (111) planes in the [111] direction; (b) AFM2: Double ferromagnetically aligned (111) Ti planes, which are antiferromagnetically aligned to the next two ferromagnetically aligned Ti(111) planes in the [111] direction.

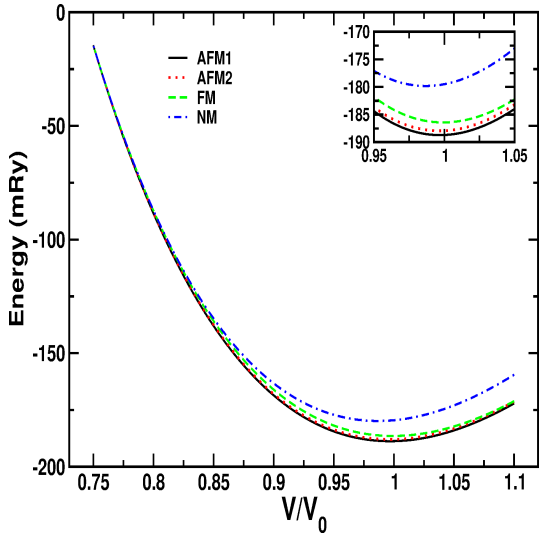

(a)

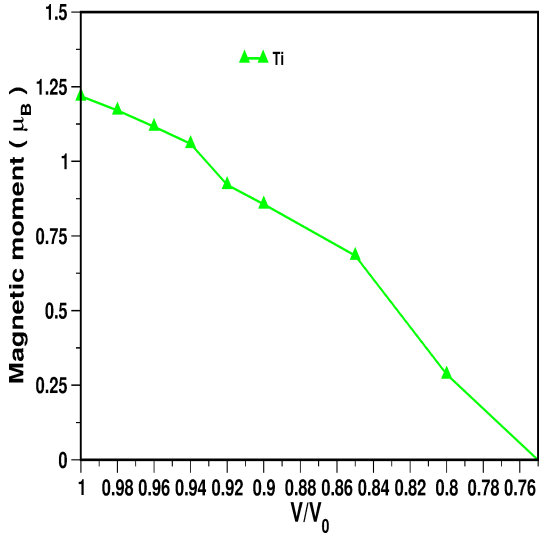

(b)

Figure 2. (a)Total energy variation with V/V_0 for Zr_2TiAl in AFM1, AFM2, Ferromagnetic and non-magnetic cases, (b) magnetic moment of Ti under compression for Zr_2TiAl.

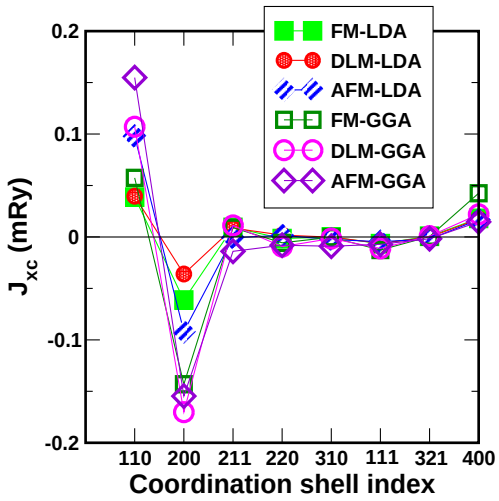

Figure 3. Magnetic exchange interactions on the Ti sublattice in Zr_2TiAl in three different states: DLM, FM, and AFM. The coordination shells are labelled by the usual fcc indices.

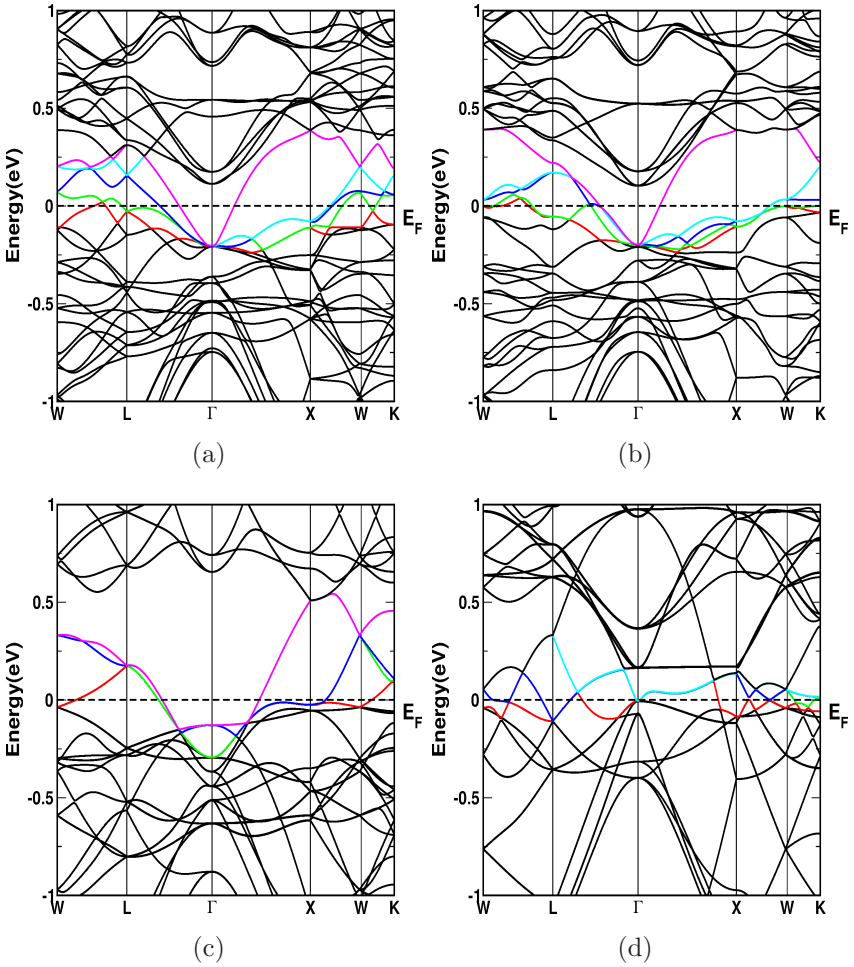

Figure 4. Band structure for Zr_2TiAl (a) at ambient AFM1 state in super cell case, (b) AFM2 state in super cell case and Ferromagnetic state in super cell case(c) majority spin (d) minority spin.

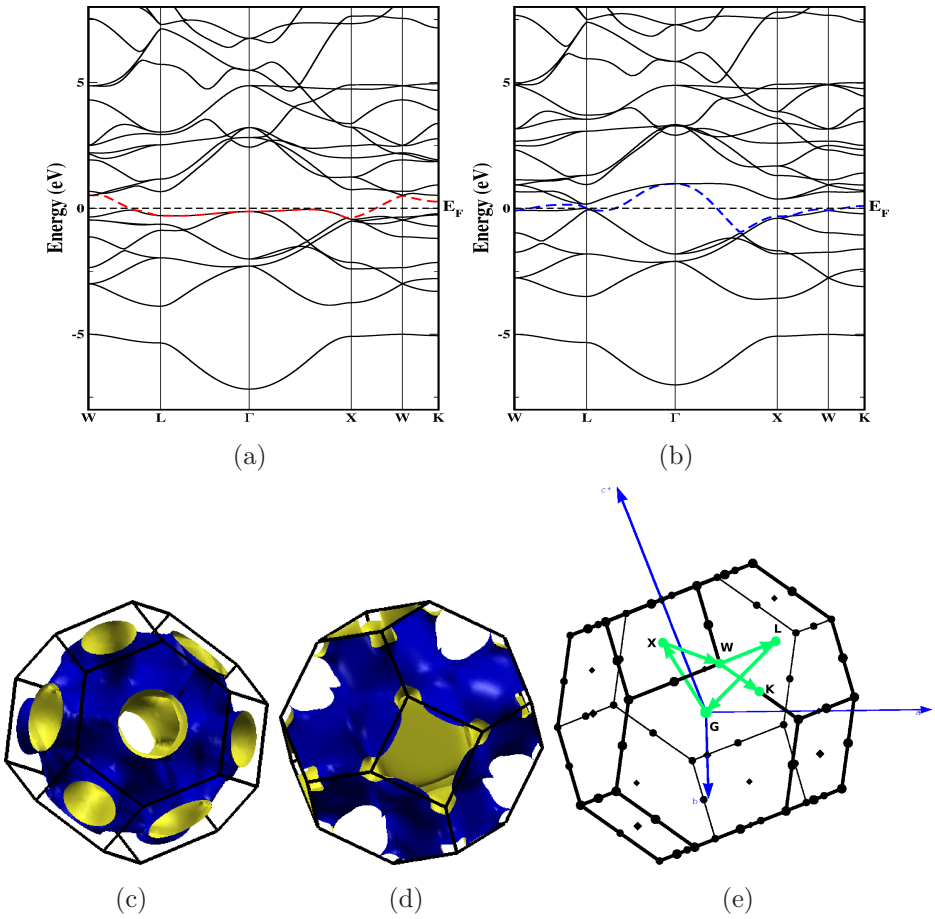

Figure 5. Band structure for Zr_2TiAl at in Ferromagnetic state without extended cell (a) majority band, (b) minority band. Fermi surface for Zr_2TiAl at Ferromagnetic state (d) majority case, (e) minority case and (f) Brillouin zone.

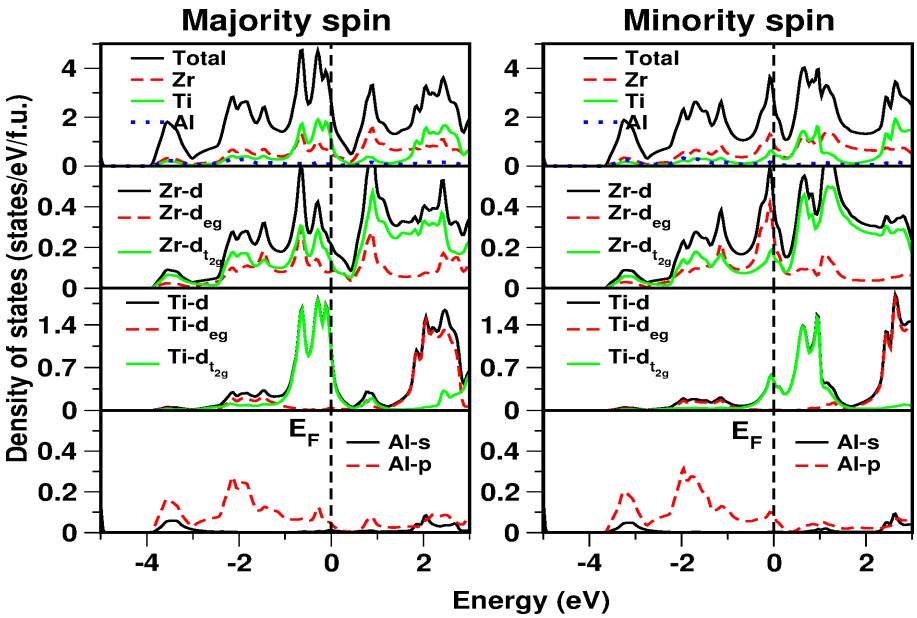

Figure 6. Density of states at ambient for Zr_2TiAl for both majority and minority spins.

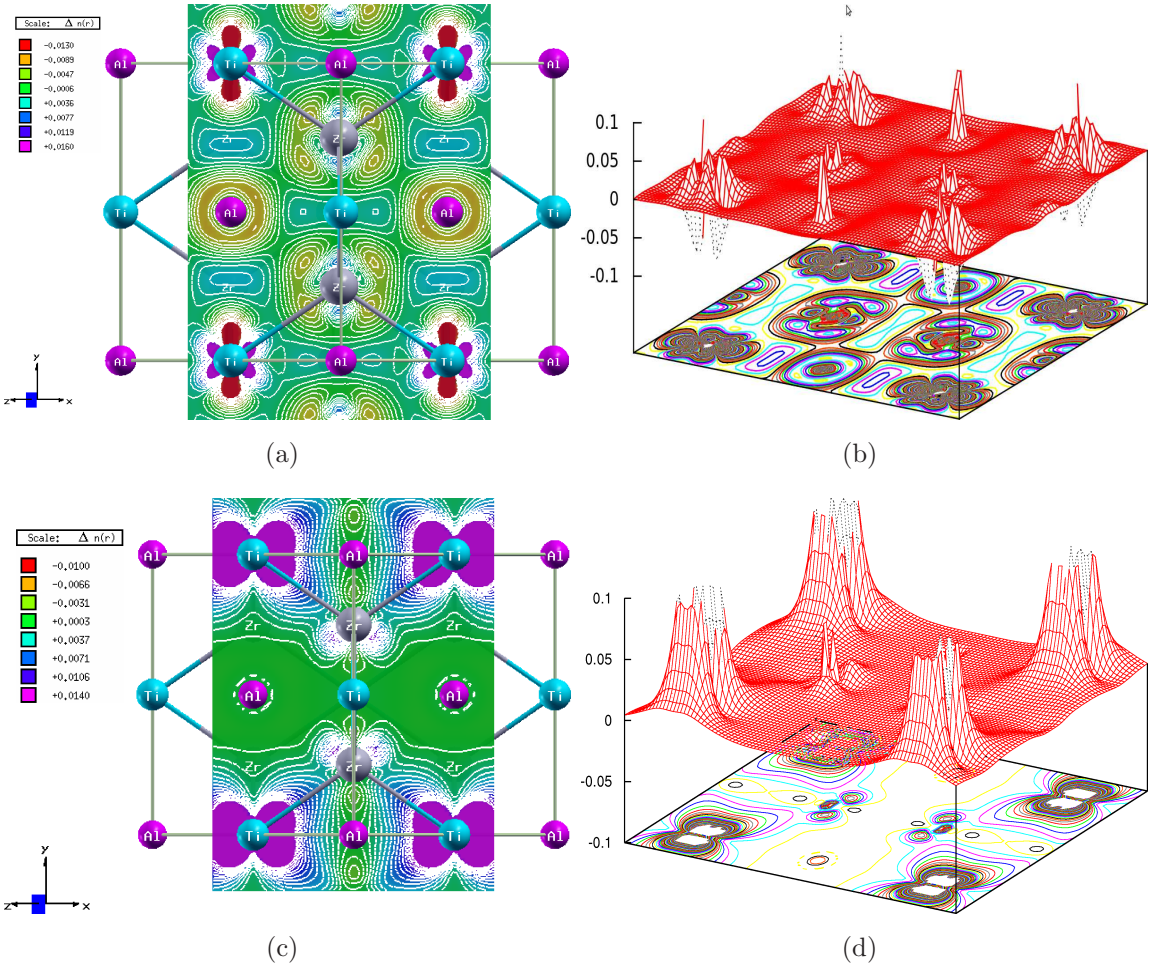

Figure 7. Difference charge density plot for Zr_2TiAl (a) in 2D and (b) in 3D spin charge density (c) in 2D and (d) in 3D.

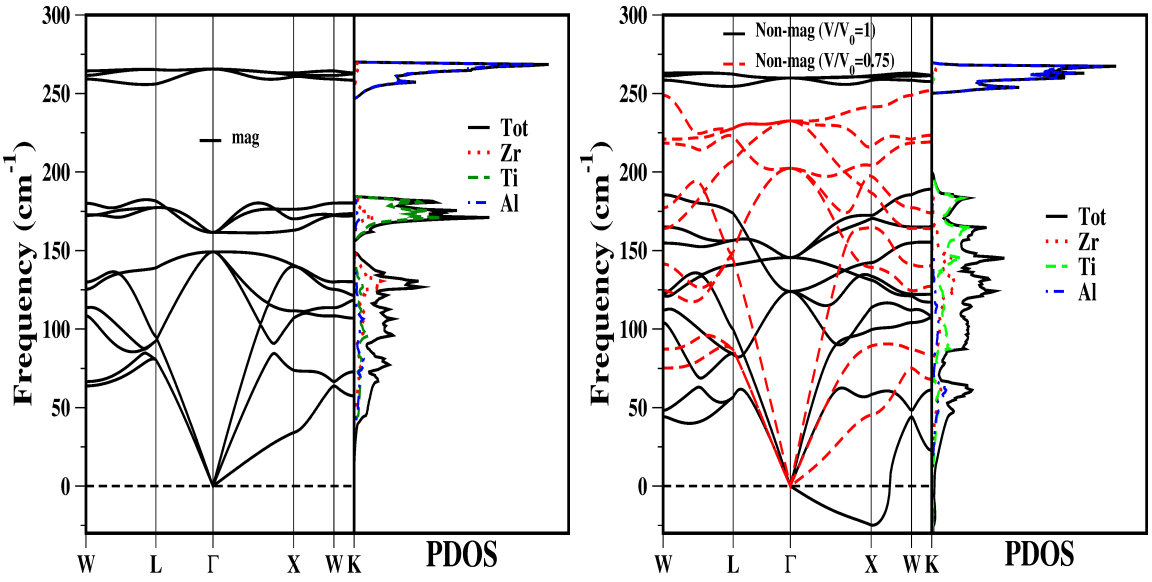

Figure 8. Phonon dispersion plots along with partial phonon density of states at ambient (a) magnetic case and (b) non magnetic case (black continuous line for V/V_0=0.1, red dotted line for V/V_0=0.75) for Zr_2TiAl.

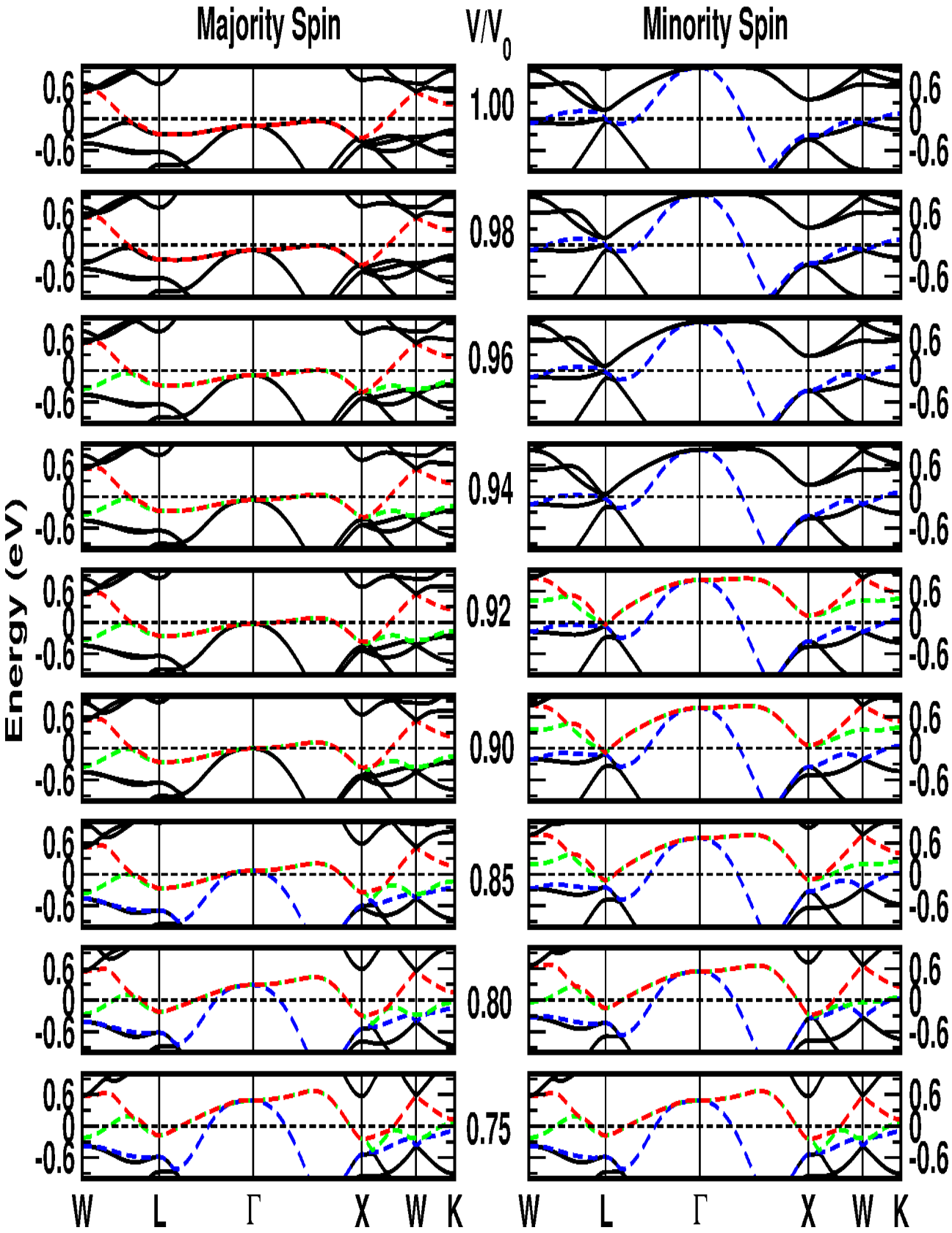

Figure 9. Band structure for Zr_2TiAl under compression is given near the vicinity of the Fermi level (0 eV). The bands which cross the E_F indicated with colour.

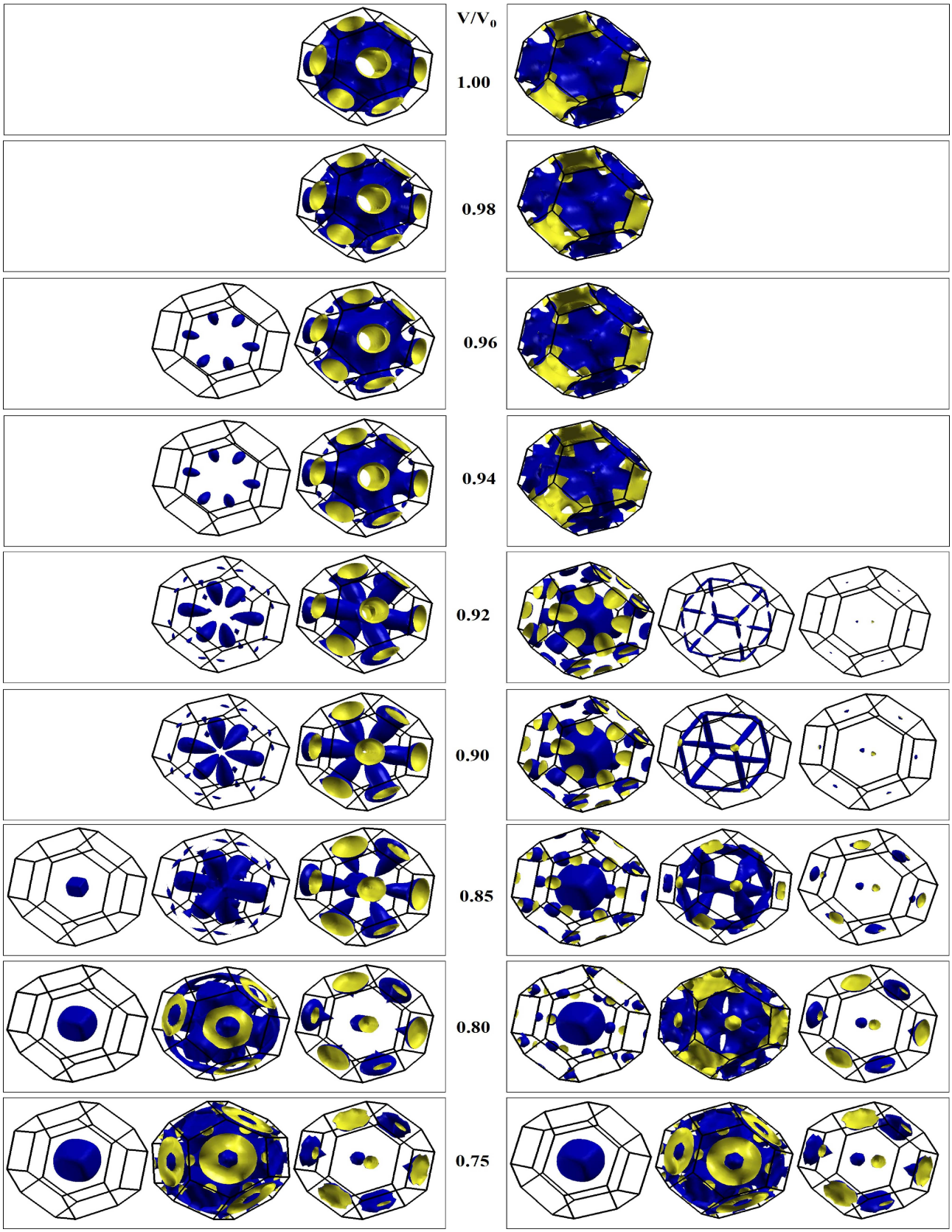

Figure 10. Fermi surface of Zr_2TiAl under compression.

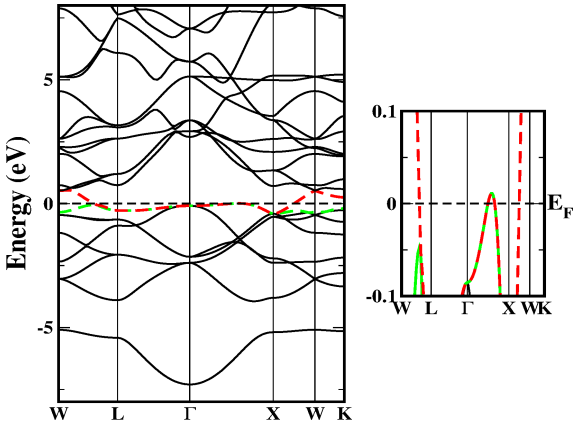

Figure 11. Majority spin band structure for Zr_2TiAl at V/V_0=0.96 (with zoom at the E_F).

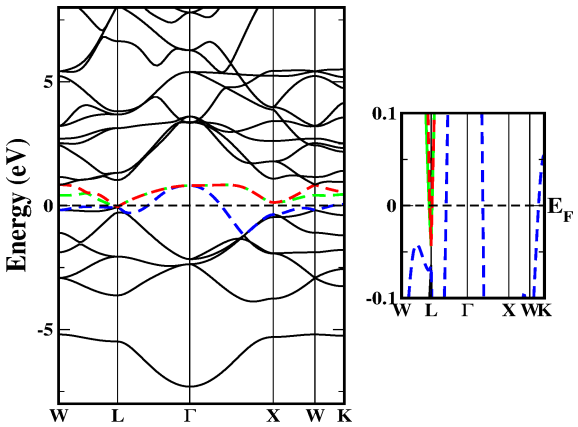

Figure 12. Minority band structure for Zr_2TiAl at V/V_0=0.92 (with zoom at the E_F).

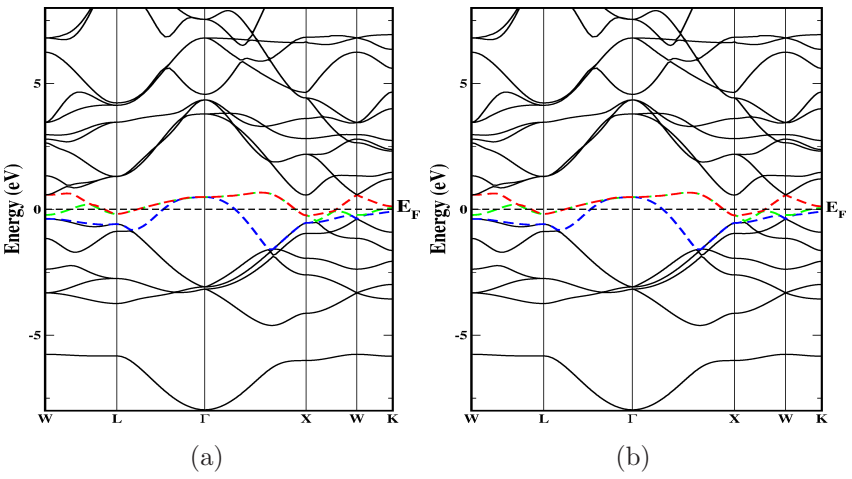

(a) (b)

Figure 13. Band structure for Zr_2TiAl at V/V_0=0.75 (a) majority spin band, (b) minority spin band.

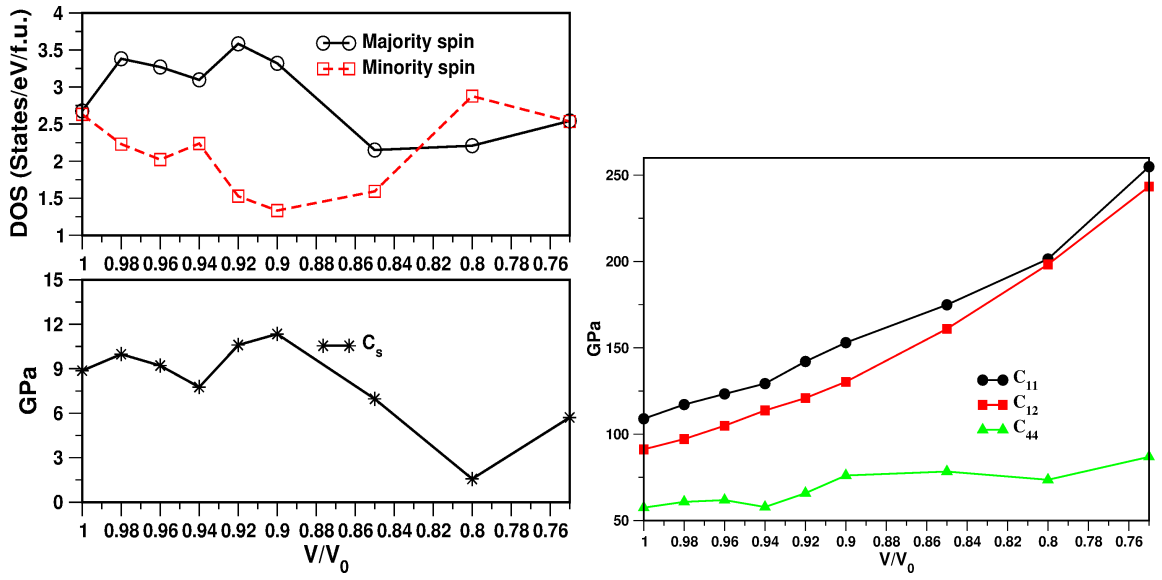

(a) (b)

Figure 14. (a)Total electronic density of states for Zr_2TiAl under compression for both majority and minority spin case along with the shear modulus (C_s) elastic constant under compression. (b) Single crystalline elastic constants under pressure.